methods

Real-time analysis of endosomal lipid transport by live cell scintillation proximity assay

Walter Stockinger, Adam B. Castoreno, Yan Wang, Joanne C. Pagnon, and Axel Nohturfft[1]

The Biolaboratories, Department of Molecular and Cellular Biology, Harvard University, Cambridge, MA 02138

Abstract **A scintillation proximity assay has been developed to study the endosomal trafficking of radiolabeled cholesterol in living cells. Mouse macrophages were cultured in the presence of tritiated cholesterol and scintillant microspheres. Microspheres were taken up by phagocytosis and stored in phagolysosomes. Absorption of tritium β particles by the scintillant produces light signals that can be measured in standard scintillation counters. Because of the short range of tritium β particles and for geometric reasons, scintillant microspheres detect only that fraction of tritiated cholesterol localized inside phagolysosomes or within a distance of ~600 nm. By incubating cultures in a temperature-controlled microplate reader, the kinetics of phagocytosis and cholesterol transport could be analyzed in near-real time. Scintillation signals were significantly increased in response to inhibitors of lysosomal cholesterol export. This method should prove a useful new tool for the study of endosomal trafficking of lipids and other molecules.**—Stockinger, W., A. B. Castoreno, Y. Wang, J. C. Pagnon, and A. Nohturfft. **Real-time analysis of endosomal lipid transport by live cell scintillation proximity assay.** ***J. Lipid Res.*** **2004.** 45: **2151–2158.**

Supplementary key words cholesterol transport • endosomes • lysosomes • macrophages • phagocytosis

Cholesterol is an essential component of cellular membranes and must be maintained at appropriate concentrations to meet the specific requirements of organelles, cells, and tissues. A multitude of mechanisms conspire to maintain cholesterol homeostasis, including cholesterol synthesis, uptake, storage, and export. Moreover, cholesterol is distributed heterogeneously among the membranes of different cellular organelles. Although the control of global cholesterol homeostasis is reasonably well understood, much less is known about the laws and mechanisms that govern intracellular cholesterol transport and sorting.

Cholesterol is synthesized from acetate or enters cells as a component of serum-derived lipoproteins by endocytosis. Lipoprotein particles such as LDL carry cholesterol predominantly as cholesteryl acyl ester that is hydrolyzed by the endosomal/lysosomal enzyme acidic cholesteryl ester hydrolase, liberating cholesterol and fatty acid (1).

In fibroblasts, two-thirds of endosomally derived cholesterol are transported to the plasma membrane and the other one-third is thought to be moved along an independent pathway to the endoplasmic reticulum (ER) (2). For both routes, the biochemical details of the transport process are unknown. Release of cholesterol from endosomes and lysosomes might involve the endosomal proteins NPC1 and NPC2, defects in which cause a lysosomal lipid storage disorder called Niemann-Pick disease type C. NPC2 directly binds cholesterol and NPC1 contains a sterol-sensing domain, a motif that confers cholesterol sensitivity to two other proteins related to cholesterol metabolism, sterol regulatory element binding protein cleavage-activating protein and 3-hydroxy-3-methylglutaryl-CoA reductase (3–5). In addition to cholesterol, however, NPC1- and NPC2-deficient cells also accumulate a number of other lipids, and it is not yet clear whether the proteins play direct, indirect, or regulatory roles in lysosomal cholesterol export.

Endosomal lipid transport in intact cells has been investigated extensively by fluorescence microscopy. These studies have relied largely on synthetic lipid analogs containing fluorescent side chains (6–11). An autofluorescent sterol, dehydroergosterol, has also proven useful as a cholesterol analog, as its movement in cells can be studied in real time with sensitive microscopic equipment (12, 13). Cholesterol and some sphingolipids have been visualized with the help of cognate bacterial protein toxins (14, 15). After cell fixation, cholesterol and other sterols can also be visualized by staining with a fluorescent polyene antibiotic called filipin (16). Transport of cholesterol to the ER has been inferred from the intracellular formation of cholesteryl esters based on the rationale that the enzyme that usually catalyzes this reaction, acyl CoA:cholesterol acyltransferase, is localized predominantly in the ER (17). Cholesterol levels at the cell surface can be measured after cell fixation based on the sensitivity of plasma mem-

Manuscript received 21 June 2004.

Published, JLR Papers in Press, August 16, 2004.
DOI 10.1194/jlr.D400011-JLR200

Abbreviations: AcLDL, acetylated LDL; CO, cholesteryl oleate; SPA, scintillation proximity assay; YSi, yttrium silicate.

[1] To whom correspondence should be addressed.
e-mail: axno@mcb.harvard.edu

brane cholesterol to exogenously added cholesterol oxidase (18). The distribution of cholesterol and lipids between different cellular compartments has also been studied through methods involving cell fractionations, mainly by density gradient centrifugation.

As an alternative approach to studying transport in the endosomal system, we have developed an in vivo scintillation proximity assay (SPA) that measures tritium levels in phagolysosomes of living cells in near-real time. This method was applied successfully to the analysis of [^{3}H]cholesterol levels in primary and immortalized mouse macrophages. Live cell SPA sensitively detected lysosomal cholesterol accumulation induced by pharmacological inhibition of cholesterol transport.

MATERIALS AND METHODS

General considerations

Katz and Penfold (19) have shown that the range of β radiation can be related to particle energy according to the equation

$$R = 412E^{1.265 - \ln(0.0954E)} \quad (Eq.\ 1)$$

where R is range in g/cm^2 and E is energy in MeV. R can be divided by the density of a given material to yield the range in units of distance. The maximum energy of tritium β particles is 18.5 keV, and the mean energy is 5.7 keV. In water, these values translate to maximum and average ranges of 5.8 and 0.47 μm, respectively. To obtain a more comprehensive view of the range/energy relationship of tritium β particles, the experimentally obtained energy spectrum of tritium (20) was converted to a cumulative probability distribution. Data points were then individually subtracted from unity to obtain the distribution that is represented by the solid line in **Fig. 1**. Using equation 1, the abscissas of this plot were converted to the corresponding range in water, which can be read off the upper x axis in Fig. 1.

Assuming linear particle propagation, the geometric contribution to the probability of an electron reaching a sphere can be expressed as

$$p(d,r) = \frac{1}{2} - \frac{\sqrt{d(d+2r)}}{2(d+r)} \quad (Eq.\ 2)$$

where d is the shortest distance between a radiation-emitting molecule and a sphere of radius r. The dashed line in Fig. 1 shows the results of this expression for the average diameter of the yttrium silicate (YSi) beads that were used in this study (2.5 μm). The contributions of distance and particle range were combined by multiplication and graphed as the dotted line in Fig. 1. It has to be emphasized that this distribution represents only the upper limit of the actual probability distribution. Especially below $d = 1$ μm, most particles that can reach a 2.5 μm sphere will travel significantly farther than d. Furthermore, at short distances, a large fraction of electrons that can reach the scintillant sphere will do so at relatively low angles, which reduces absorption efficiency.

Materials

We obtained egg yolk phosphatidylcholine (P-2772), dioleoyl phosphatidylserine (P-1060), dicetyl phosphate, cytochalasin B (C-6762), cytochalasin D (C-8273), latrunculin A (L-5163), and progesterone (P-8783) from Sigma; [1,2-^{3}H(N)]cholesterol (NET-139) and [1,2,6,7-^{3}H(N)]cholesteryl oleate ([^{3}H]CO; NET-746) were from Perkin-Elmer; YSi and polyvinyltoluene scintillating beads were from Amersham; FBS was from Invitrogen; other cell culture reagents were from Mediatech. Cytochalasins and latrunculin A were dissolved in DMSO and stored as 1,000× stock solutions at −20°C. Progesterone was dissolved in ethanol and stored at 4°C. Lipoprotein-deficient FBS and LDL were prepared as described (21). Acetylated LDL (AcLDL) was prepared (22) and reconstituted with [^{3}H]CO (0.5 mg/ml, 120 μCi/mg) (23) as described in the indicated references. Anionic liposomes were prepared as described (24) and contained 1 mM phosphatidylcholine, 1 mM phosphatidylserine, 0.2 mM dicetyl phosphate plus [^{3}H]cholesterol or [^{3}H]CO as indicated in the figure legends.

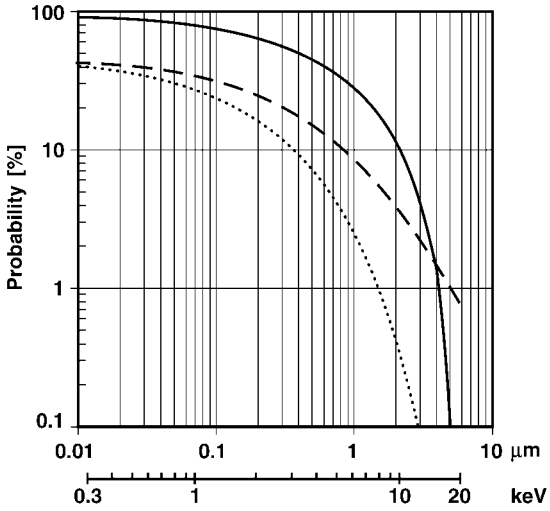

Fig. 1. Theoretical probability distributions of the range of tritium β particles. Distributions were determined as described in Materials and Methods. The upper x axis represents distance in micrometers and the axis below represents energy in kiloelectron volts. The distance scale is related to the energy scale according to equation 1. All scales are decimal logarithmic. The solid line ordinates indicate the probability of tritium β particles having a kinetic energy greater than the corresponding abscissas on the keV scale as well as the probability of tritium β particles traveling farther in water than the corresponding abscissas on the μm scale. The dashed line was generated with equation 1 for a radius of 1.25 μm and indicates the probability of a linearly propagating particle reaching a sphere with a diameter of 2.5 μm as a function of the shortest distance between the particle's origin and the sphere. The dotted line was generated by multiplication of discrete probability values from the preceding two data sets and gives an estimate for the probability of tritium β particles reaching a 2.5 μm sphere as a function of distance.

Cell culture

J774 mouse macrophages were grown in monolayer culture at 37°C in an atmosphere of 8–9% CO_2 in medium A (a 1:1 mixture of Ham's F-12 medium and Dulbecco's modified Eagle medium plus 100 U/ml penicillin, 100 μg/ml streptomycin sulfate, and 10% [v/v] FBS).

Mouse peritoneal macrophages

Balb/c mice were housed in colony cages, maintained on a 12 h light/12 h dark cycle, and fed a regular chow diet. Peritoneal macrophages were elicited by injection with Biogel P-100 (Bio-Rad) of 40 day old mice as described (25). Four days later, mice were killed and 3 ml of PBS was injected into the peritoneal cavity, withdrawn, and collected. PBS injection was repeated twice and the fluids pooled. Cells were pelleted at 1,000 g for 5 min

and resuspended in 3 ml of red blood cell lysis buffer (10 mM potassium bicarbonate, 155 mM ammonium chloride, and 0.1 mM EDTA, pH 7.4). After 3 min at room temperature, cells were washed once in PBS and resuspended in medium B (phenol red-free Dulbecco's modified Eagle medium, 50 mM Hepes, 2 mM L-glutamine, 100 U/ml penicillin, 100 μg/ml streptomycin sulfate, and 10% FBS). Cells were counted and plated as detailed in the figure legends.

In vivo SPA

Cells were set up in opaque 24-well plates (Packard) at the indicated densities in 0.5 ml of medium B per well. Plates were sealed with transparent plastic foil. In vivo readings were performed in a Topcount-NXT microplate scintillation counter (Packard) equipped with two 24-well format photomultiplier tubes. Nuclide settings in the instrument control software were as follows: scintillator, glass; energy range, low; efficiency mode, high sensitivity; region A, 0–50; region B, 0–256. Wells were read for 30 s at a time. The instrument was connected to a circulating-water bath to keep the temperature in the counting chamber constant at 33°C.

RESULTS

We initially tested whether scintillant beads could be used to study [^{3}H]cholesterol levels in intracellular membranes of living macrophages. The approach is based on the principles of SPA, which has been used extensively for studies on receptor/ligand-type interactions (26, 27). SPA is based in part on the fact that low-energy β particles have a high propensity to interact with matter and thus propagate only short distances. One isotope that is often used for SPA is tritium, which emits β particles with maximum and average ranges in water of 5.7 and 0.47 μm, respectively. If decaying atoms are localized in sufficient proximity to a scintillating microsphere, electron absorption by the scintillant may lead to photon emission, which can be detected by a scintillation counter. In addition to the energy spectrum of the isotope, geometric constraints also limit the effective radius that can be sampled by scintillant microspheres. For example, a β particle produced on the surface of a scintillant microsphere has only a 50% chance of causing excitation. For a 2.5 μm sphere, this probability is reduced to ~10% at a distance of 0.85 μm. If 2.5 μm scintillant spheres are immersed in a homogenously distributed solution of a tritium-containing compound and energetic and geometric considerations are combined, it can be estimated that more than 95% of the resulting fluorescence will derive from tritium atoms within a radius of 600 nm (Fig. 1; see Materials and Methods for details).

The YSi scintillant particles that were used in this study are on average 2.5 μm in diameter and are thus of a convenient size to be phagocytosed by macrophages. If macrophage membranes also contained tritium-labeled cholesterol, we reasoned, scintillation measurements should reflect the amount of [^{3}H]cholesterol in the immediate vicinity of intracellular beads. In such a system, the specificity of the signal should be enhanced by the fact that cellular cholesterol, as a result of its virtual insolubility in water, is found almost exclusively in membranes. We initially chose to work with mouse J774 cells, a macrophage cell line that has been widely used as a model of atherosclerotic foam cells and in studies on phagocytosis. Tritium-labeled cholesterol or cholesteryl esters can be delivered to J774 cells and other macrophages by packaging the lipids in lipoprotein particles such as oxidized LDL or AcLDL or in liposomes (23, 24). Both AcLDL and anionic liposomes are efficiently internalized via macrophage scavenger receptors (28, 29).

For the experiment in **Fig. 2A**, J774 cells were incubated with AcLDL as a source of [^{3}H]CO plus increasing amounts of YSi beads. The cultures were then placed in a microplate reader at 33°C to record the scintillation signal. Scintillation gradually increased over time, reflecting the uptake of AcLDL, the phagocytosis of beads, and the movement of tritium-labeled lipids into the vicinity of the scintillant. At 20 h, the scintillation signal was linearly proportional to the amount of beads ($r^2 > 0.999$) (Fig. 2A, inset).

Next, we sought to determine how the in vivo scintillation signal responds to varying concentrations of [^{3}H]cholesterol. J774 macrophages were incubated with YSi beads plus increasing amounts of [^{3}H]CO-containing AcLDL, and the scintillation signal was recorded over a period of 20 h (Fig. 2B). A plot of the scintillation signal at 20 h versus the AcLDL concentration resulted in a straight line ($r^2 > 0.999$), indicating that the readout at steady state is directly proportional to the amount of radioactive lipids present (Fig. 2C). The AcLDL concentrations used in this experiment are well within the range typically used to study cholesterol metabolism in macrophages (e.g., Ref. 30).

All time-resolved traces shown in this study were derived by averaging the readings from multiple, identically treated wells. To illustrate the degree of variation associated with the assay in Fig. 2B, coefficients of variation are plotted as a function of the standard deviation for two representative curves (Fig. 2D). Average coefficients of variation for all traces in Fig. 2B varied between ~3% and 15% but showed no significant correlation with AcLDL concentration, indicating that the assay-associated error scales with the scintillation signal (Fig. 2D, inset).

An added advantage of using phagocytes to study lipid transport in the endosomal system is the possibility of harvesting macrophages from the peritoneum or bone marrow of mice (25). Because a growing number of mouse models for lysosomal storage diseases are becoming available (31), live cell SPA can thus be combined with genetics to study the mechanisms of endosomal lipid transport and sorting. To test the feasibility of this approach, peritoneal macrophages from Balb/c mice were cultured for 24 h in the presence of [^{3}H]CO-containing AcLDL to allow the [^{3}H]cholesterol content of the cells to reach steady state. The AcLDL was then removed, YSi beads were added, and the scintillation signal was recorded. As shown in **Fig. 3A** (control trace), the signal rapidly increased over time and reached steady state at eight times the initial value after ~2.5 h. Mouse peritoneal macrophages thus represent an excellent cell system for live cell SPA. Results similar to those shown in Fig. 3A were obtained with J774 cells (data not shown).

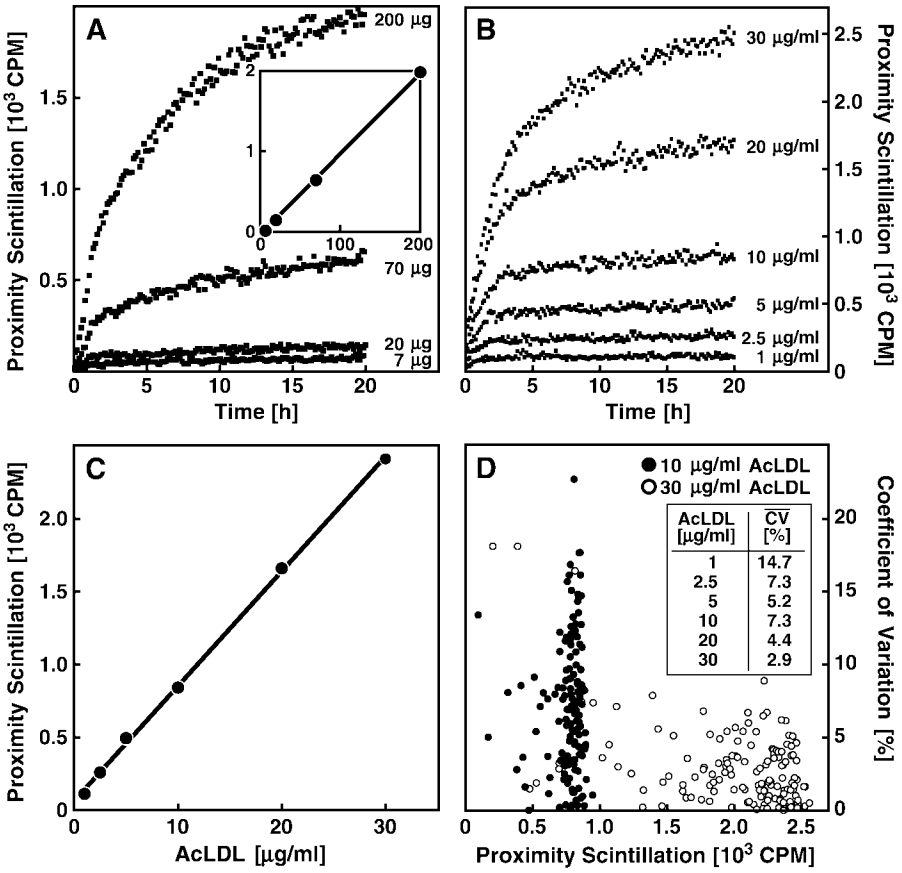

Fig. 2. Live cell scintillation proximity assay. A: J774 macrophages were set up at 2×10^6 cells per well in medium B and supplemented with 6.5 µg/ml acetylated LDL {AcLDL; reconstituted with [1,2,6,7-^{3}H(N)]cholesteryl oleate ([^{3}H]CO); 160 µCi/mg protein} plus the indicated amount of yttrium silicate (YSi) beads per well. Proximity scintillation was recorded at 33°C over a period of 20 h. Each time point represents the average of two wells. Average coefficients of variation were 15% (7 µg/ml), 22% (20 µg/ml), 11% (70 µg/ml), and 3% (200 µg/ml). The inset shows the average proximity scintillation of the last five time points of each curve in A plotted as a function of the amount of beads per well ($r^2 = 0.9986$). SD values ranged from 3 to 34 cpm and are smaller than the symbols. B: J774 macrophages were set up at 2×10^6 cells/well in medium B and supplemented with 100 µg of YSi beads plus the indicated concentrations of AcLDL (reconstituted with [^{3}H]CO; 120 µCi/mg protein). Each time point represents the average of four wells. C: The average proximity scintillation of the last five time points of each curve in B is plotted as a function of the AcLDL concentration ($r^2 = 0.9993$). SD values varied from 14 to 50 cpm and are smaller than the symbols. D: For the 10 and 30 µg/ml AcLDL traces in B, the coefficients of variation are plotted as a function of the SD of each data point. The inset shows the average coefficient of variation (CV) for each curve in A.

In the experiments shown in Fig. 3 (A and B), we also asked whether the scintillation signal observed with living macrophages was in fact dependent on phagocytosis. To address this question, phagocytosis inhibitors were added to cultures soon before the addition of scintillant beads. In the presence of cytochalasin D (32), the scintillation signal did not significantly increase above background and remained at ~20% of control values at steady state (Fig. 3A). Similar results were obtained with two other phagocytosis inhibitors, cytochalasin B and latrunculin A (Fig. 3B) (33, 34). Scintillation was reduced to almost zero when detergent was added to the cultures (data not shown). These results indicate that maximally 20% of the scintillation signal derives from external beads in proximity with the cell surface.

Comparison of the traces in Fig. 2A and Fig. 3A illustrates that the initial slope of the traces are higher and that the scintillation signal reaches equilibrium significantly earlier when cells are loaded with [^{3}H]CO first and then supplied with beads at a later stage. Under the latter conditions, [^{3}H]cholesterol will have equilibrated among cellular membranes before phagocytosis is started, the majority being in the plasma membrane (2). In such an experimental setup, scintillation initiates with patches of plasma membrane wrapping around the beads during the earliest phases of particle uptake. The early time points in Fig. 3A can thus be considered to represent the kinetics of the phagocytosis process, whereas the scintillation signal at later stages reflects the steady-state distribution of [^{3}H]cholesterol in intracellular membranes.

To confirm that [^{3}H]cholesterol in phagosomal membranes contributes to the scintillation signal, we performed

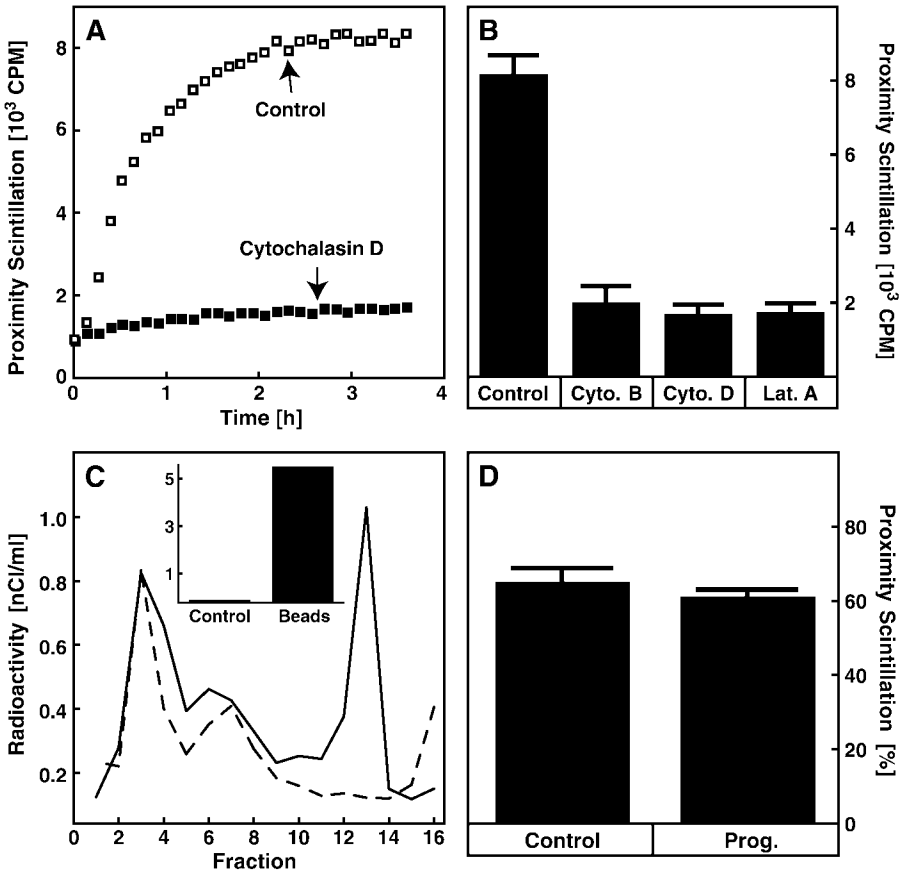

Fig. 3. Phagocytosis dependence of in vivo proximity scintillation. A and B: On day 0, mouse peritoneal macrophages were set up at 10^6 cells per well in medium A. On day 1, cells were switched to medium A plus 10 μg/ml AcLDL (reconstituted with [^{3}H]CO; 120 nCi/mg protein) and incubated at 37°C for 24 h. On day 2, cells were switched to medium B plus 0.1% DMSO and 100 μM cytochalasin B (Cyto. B), 20 μM cytochalasin D (Cyto. D), or 0.5 μM latrunculin A (Lat. A) as indicated. After 30 min at 37°C, 150 μg of YSi beads was added to each well, and cells were incubated on ice for 30 min to allow the beads to settle. Subsequently, the dish was moved to a microplate scintillation counter at 33°C to initiate proximity scintillation readings. A: Time-resolved proximity scintillation of cells incubated in the absence or presence of cytochalasin D. Data points represent the average of four identically treated wells. Average coefficients of variation were 11% (control) and 16% (cytochalasin D). B: Proximity scintillation after 5 h in the presence of the indicated inhibitors. Error bars indicate SD (n = 5). C and D: On day 0, two dishes of J774 cells were set up at 25% confluence in medium A. On day 1, cells were switched to medium A plus [^{3}H]CO-containing liposomes (1 nCi/ml medium) and incubated overnight. On day 2, 25 mg of scintillant polyvinyltoluene (PVT) beads were added to one dish and cells were allowed to phagocytose for 4 h. Then, cells were washed and harvested. Cells from the control dish were mixed with 25 mg of PVT beads after harvest. Cells were overlaid with a continuous 0–30% sucrose gradient and centrifuged for 2 h at 40,000 rpm. One milliliter fractions were collected, and total radioactivity and bead concentration were determined. C: Total radioactivity in individual fractions as determined by liquid scintillation counting. Dashed line, control; solid line, beads internalized by phagocytosis. The inset shows proximity scintillation in fraction 13 corrected for bead concentration (cpm/mg PVT). D: J774 cells were set up as in C and incubated with [^{3}H]CO in the absence (Control) or presence (Prog.) of 10 μg/ml of progesterone as indicated. The cells were then incubated with PVT beads (6 mg/dish) for 4 h. Proximity scintillation and total radioactivity were determined before and after cell fractionation. Data represent the ratio of proximity scintillation in the peak bead-containing fraction versus proximity scintillation in intact cells before fractionation. Error bars indicate SD (n = 2).

the experiment shown in Fig. 3C. First, J774 cells were equilibrated with [^{3}H]cholesterol overnight. Subsequently, cells received scintillant latex beads for 4 h and were then subjected to density gradient centrifugation. As a control, some radiolabeled cells received an equivalent amount of beads immediately before centrifugation. Individual gradient fractions were analyzed for the presence of beads, for proximity scintillation, and for the amount of total radioactivity. Both in control samples and in lysates from cells that had internalized the scintillant by phagocytosis, most of the beads were found as a sharp band in fraction 13 (data not shown). In this fraction, however, appreciable amounts of radioactivity (Fig. 3C, main panel) and proximity scintillation (Fig. 3C, inset) were only detected in samples that had internalized the beads by phagocytosis. These data indicate that [^{3}H]cholesterol is present in

the phagosomal membrane and that it is detected by scintillation proximity measurements.

To estimate what fraction of the live-cell proximity scintillation signal is derived from [^{3}H]cholesterol in the phagosomal membrane versus [^{3}H]cholesterol in other cellular compartments, we measured proximity scintillation in intact cells and then again after fractionation of the same samples by density gradient centrifugation. Approximately 60% of the scintillation signal was recovered from phagosomes (Fig. 3D). The bead-containing fraction contained 3.3% and 3.5% of total cellular β-hexosaminidase and acidic β-galactosidase activity, respectively, confirming that these vesicles had matured into phagolysosomes. The phagolysosomal fraction contained only 1% of the total cytosolic lactate dehydrogenase activity and no detectable activity of the plasma membrane enzyme 5′-nucleotidase, indicating that it contained very few intact cells (data not shown). Taken together, the results in Fig. 3 (A–C) can be summarized to indicate that 20% of the proximity scintillation signal obtained with living cells at steady state is derived from extracellular beads, 60% of the signal reflects tritiated lipids in phagosomes, and 20% represents radioactivity in nonphagosomal vesicles. Because the signal in the presence of phagocytosis inhibitors did not significantly increase beyond the value at time zero, values adjusted by subtraction of the background specifically reflect intracellular material. Based on these considerations, it can be estimated that at steady state, 75% of background-corrected data reflect phagosomal radiolipids.

Several small molecules, including progesterone and U18666A, have been shown to cause accumulation of cholesterol in lysosomes (2). To determine whether this effect could be quantified by live-cell SPA, J774 cells were cultured for 16 h with [^{3}H]CO-containing AcLDL and YSi beads plus or minus progesterone. The cells were then harvested to determine bead-derived scintillation, total cel-

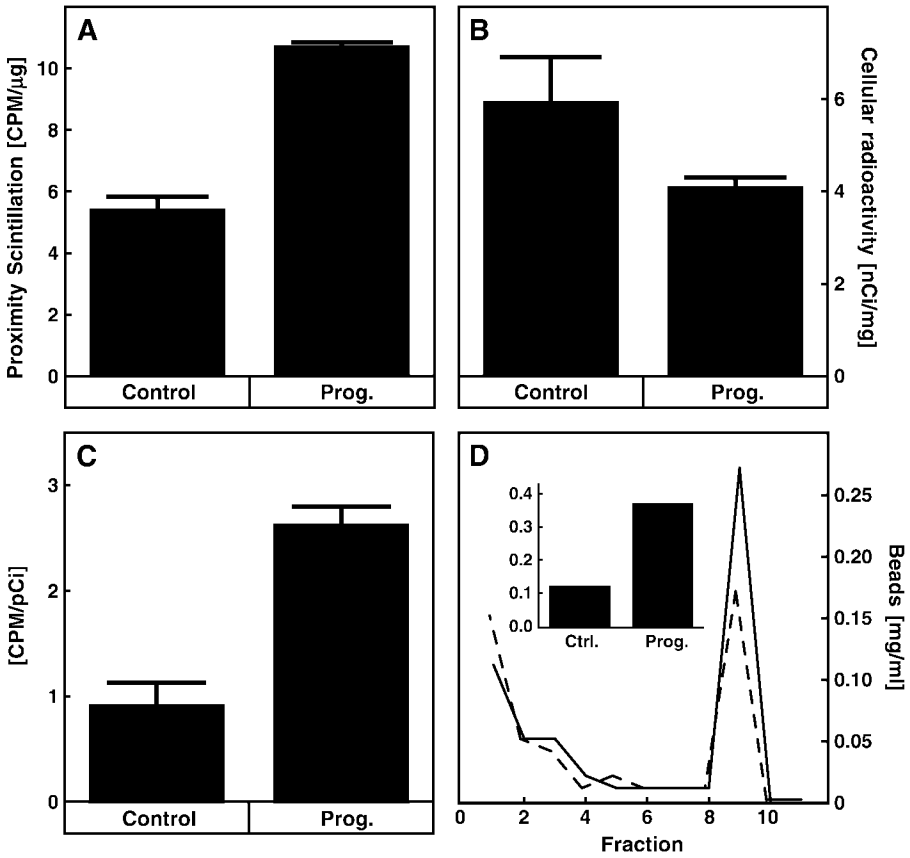

Fig. 4. Effect of progesterone (Prog.) on proximity scintillation. A–C: J774 macrophages were set up at 10^7 cells in 10 cm dishes in medium A. After 16 h, each dish received 1 mg of YSi beads, 10 μg/ml AcLDL (reconstituted with [^{3}H]CO; 120 μCi/mg protein), and 0.1% ethanol with or without 10 μg/ml progesterone as indicated. After 16 h, cells were washed three times with PBS, scraped into 1 ml of PBS, and transferred to 20 ml scintillation vials. A: Proximity scintillation corrected for cellular protein concentration. B: After proximity scintillation readings, vials received liquid scintillation cocktail to determine total cellular radioactivity. C: Values represent the ratio of bead-derived scintillation in A divided by the total cellular radioactivity in B. Error bars indicate SD (n = 2). D: On day 0, two dishes of J774 cells were set up at 25% confluence in medium A. On day 1, cells were switched to medium A with [^{3}H]CO-containing liposomes (1 nCi/ml medium) in the absence or presence of 10 μg/ml progesterone and incubated overnight. Cells then received 25 mg of PVT beads for 2 h. Subsequently, samples were subjected to 0–30% sucrose gradient centrifugation. Data indicate bead concentrations in individual gradient fractions. The inset shows total radioactivity normalized for bead concentration in fraction 9.

lular radioactivity (by liquid scintillation counting), and protein concentration. The specific bead-derived scintillation signal emanating from intact cells was ~2-fold higher in progesterone-treated samples compared with controls (**Fig. 4A**). Total cellular amounts of tritiated lipids were slightly lower in progesterone-treated samples (Fig. 4B), such that the ratio of the bead-derived scintillation signal over total cellular radioactivity was ~2.8-fold higher in progesterone-treated versus nontreated samples (Fig. 4C). Treatment of primary mouse peritoneal macrophages with either progesterone or U18666A also led to an increase of the scintillation signal (data not shown).

To verify whether the increased scintillation signal in response to progesterone in fact reflected higher concentrations of [^{3}H]cholesterol in phagosomes, cells were loaded with [^{3}H]CO and scintillant beads and then fractionated by density gradient centrifugation. As shown in Fig. 4D (main panel), a large fraction of the beads concentrated in a single peak near the top of the gradient in fraction 9. In this fraction, the total amount of radioactivity (as determined by liquid scintillation counting) corrected for the amount of beads was 2.5-fold higher in progesterone-treated samples compared with controls (Fig. 4D, inset). These results demonstrate that SPA can be used to detect drug-induced cholesterol accumulation in phagosomes of living cells.

DISCUSSION

We have demonstrated the usefulness of scintillant microspheres to measure [^{3}H]cholesterol levels in cellular membranes of living cells. YSi microspheres enter macrophages by phagocytosis and are stored in phagolysosomes. Absorption of [^{3}H]cholesterol-derived β particles by the scintillant leads to photon emission that can be measured with photomultiplier tubes.

Macrophages can be kept in common glass scintillation vials and then analyzed in a standard scintillation counter. Alternatively, cells can be grown on multiple-well plates that require appropriately equipped scintillation readers with horizontally adjustable photomultiplier tubes. The latter setup, in combination with a temperature-controlled counting chamber, offers the opportunity of continuous data collection with actively metabolizing cells. The method thus offers an alternative approach to kinetic analyses of phagocytosis and of lipid flux through the endosomal system.

As a consequence of the low energy of tritium β particles and because of geometric constraints, scintillant microspheres can effectively detect only that fraction of [^{3}H]cholesterol that is localized within a distance of ~600 nm. Through the use of phagocytosis inhibitors and cell fractionation, we were able to estimate that ~75% of the scintillation signal at steady state derives from [^{3}H]cholesterol within the confines of phagosomal membranes (Fig. 3).

Detailed studies of the protein composition of latex bead-containing phagosomes have confirmed the notion that the composition of mature phagolysosomes is very similar to that of lysosomes (35). Here, we show that phagolysosomes, like lysosomes, accumulate excess amounts of [^{3}H]cholesterol after incubation of cells with the cholesterol transport inhibitor progesterone (Fig. 4). Similar results were obtained with U18666A, a hydrophobic amine that is also known to cause cholesterol buildup in lysosomal vesicles (data not shown). Accumulation of [^{3}H]cholesterol in phagolysosomes was indicated by an increase of proximity scintillation readings and confirmed by cell fractionation studies (Fig. 4). Measurement of tritiated molecules by live-cell SPA thus offers a viable new method to study lysosomal trafficking, especially in cases in which the use of authentic and unmodified analytes is essential. This technique might prove particularly useful in studies of lysosomal storage disorders and for kinetic modeling approaches.

The authors thank F. Engert, Y.K. Ho, and V. Murthy for stimulating discussions. The current work was supported by grants from the National Institutes of Health (DK-59934) and the Ara Parseghain Medical Research Foundation. W.S. was supported by a fellowship from the Max Kade Foundation.

REFERENCES

1. Assmann, G., and U. Seedorf. 2001. Acid lipase deficiency: Wolman disease and cholesteryl ester storage disease. *In* The Metabolic and Molecular Bases of Inherited Disease. C. R. Scriver, A. L. Beaudet, D. Valle, and W. S. Sly, editors. McGraw-Hill, New York. 3551–3572.
2. Liscum, L., and N. J. Munn. 1999. Intracellular cholesterol transport. *Biochim. Biophys. Acta.* **1438:** 19–37.
3. Carstea, E. D., J. A. Morris, K. G. Coleman, S. K. Loftus, D. Zhang, C. Cummings, J. Gu, M. A. Rosenfeld, W. J. Pavan, D. B. Krizman, J. Nagle, M. H. Polymeropoulos, S. L. Sturley, Y. A. Ioannou, M. E. Higgins, M. Comly, A. Cooney, A. Brown, C. R. Kaneski, E. J. Blanchette-Mackie, N. K. Dwyer, E. B. Neufeld, T. Y. Chang, L. Liscum, J. F. Strauss, K. Ohno, M. Zeigler, R. Carmi, J. Sokol, D. Markie, R. R. O'Neill, O. P. van Diggelen, M. Elleder, M. C. Patterson, R. O. O'Brady, M. T. Vanier, P. G. Pentchev, and D. A. Tagle. 1997. Niemann-Pick C1 disease gene: homology to mediators of cholesterol homeostasis. *Science.* **277:** 228–231.
4. Sever, N., T. Yang, M. S. Brown, J. L. Goldstein, and R. A. DeBose-Boyd. 2003. Accelerated degradation of HMG CoA reductase mediated by binding of Insig-1 to its sterol-sensing domain. *Mol. Cell.* **11:** 25–33.
5. Yang, T., P. J. Espenshade, M. E. Wright, D. Yabe, Y. Gong, R. Aebersold, J. L. Goldstein, and M. S. Brown. 2002. Crucial step in cholesterol homeostasis: sterols promote binding of SCAP to INSIG-1, a membrane protein that facilitates retention of SREBPs in ER. *Cell.* **110:** 489–500.
6. Pagano, R. E., and C. S. Chen. 1998. Use of BODIPY-labeled sphingolipids to study membrane traffic along the endocytic pathway. *Ann. N. Y. Acad. Sci.* **845:** 152–160.
7. Alecio, M. R., D. E. Golan, W. R. Veatch, and R. R. Rando. 1982. Use of a fluorescent cholesterol derivative to measure lateral mobility of cholesterol in membranes. *Proc. Natl. Acad. Sci. USA.* **79:** 5171–5174.
8. Grechishnikova, I. V., F. Bergstrom, L. B. Johansson, R. E. Brown, and J. G. Molotkovsky. 1999. New fluorescent cholesterol analogs as membrane probes. *Biochim. Biophys. Acta.* **1420:** 189–202.
9. Sparrow, C. P., S. Patel, J. Baffic, Y. S. Chao, M. Hernandez, M. H. Lam, J. Montenegro, S. D. Wright, and P. A. Detmers. 1999. A fluorescent cholesterol analog traces cholesterol absorption in hamsters and is esterified in vivo and in vitro. *J. Lipid Res.* **40:** 1747–1757.
10. Scheidt, H. A., P. Muller, A. Herrmann, and D. Huster. 2003. The potential of fluorescent and spin-labeled steroid analogs to mimic natural cholesterol. *J. Biol. Chem.* **278:** 45563–45569.
11. Wiegand, V., T. Y. Chang, J. F. Strauss 3rd, F. Fahrenholz, and G.

Gimpl. 2003. Transport of plasma membrane-derived cholesterol and the function of Niemann-Pick C1 Protein. *FASEB J.* **17:** 782–784.
12. Schroeder, F. 1984. Fluorescent sterols: probe molecules of membrane structure and function. *Prog. Lipid Res.* **23:** 97–113.
13. Mukherjee, S., X. Zha, I. Tabas, and F. R. Maxfield. 1998. Cholesterol distribution in living cells: fluorescence imaging using dehydroergosterol as a fluorescent cholesterol analog. *Biophys. J.* **75:** 1915–1925.
14. Sugii, S., P. C. Reid, N. Ohgami, Y. Shimada, R. A. Maue, H. Ninomiya, Y. Ohno-Iwashita, and T. Y. Chang. 2003. Biotinylated theta-toxin derivative as a probe to examine intracellular cholesterol-rich domains in normal and Niemann-Pick type C1 cells. *J. Lipid Res.* **44:** 1033–1041.
15. Schiavo, G., and F. G. van der Goot. 2001. The bacterial toxin toolkit. *Nat. Rev. Mol. Cell Biol.* **2:** 530–537.
16. Norman, A. W., R. A. Demel, B. de Kruyff, and L. L. van Deenen. 1972. Studies on the biological properties of polyene antibiotics. Evidence for the direct interaction of filipin with cholesterol. *J. Biol. Chem.* **247:** 1918–1929.
17. Khelef, N., T. T. Soe, O. Quehenberger, N. Beatini, I. Tabas, and F. R. Maxfield. 2000. Enrichment of acyl coenzyme A:cholesterol O-acyltransferase near trans-Golgi network and endocytic recycling compartment. *Arterioscler. Thromb. Vasc. Biol.* **20:** 1769–1776.
18. Lange, Y. 1992. Tracking cell cholesterol with cholesterol oxidase. *J. Lipid Res.* **33:** 315–321.
19. Katz, L., and A. S. Penfold. 1952. Range-energy relations for electrons and the determination of beta-ray end-point energies by absorption. *Rev. Mod. Phys.* **24:** 28–44.
20. Cooper, E. P., and F. T. Rogers. 1950. Composite of experimental measurements of the energy-distribution among beta-particles from tritium. *Phys. Rev.* **77:** 402–403.
21. Goldstein, J. L., S. K. Basu, and M. S. Brown. 1983. Receptor-mediated endocytosis of low-density lipoprotein in cultured cells. *Methods Enzymol.* **98:** 241–260.
22. Basu, S. K., J. L. Goldstein, G. W. Anderson, and M. S. Brown. 1976. Degradation of cationized low density lipoprotein and regulation of cholesterol metabolism in homozygous familial hypercholesterolemia fibroblasts. *Proc. Natl. Acad. Sci. USA.* **73:** 3178–3182.
23. Krieger, M. 1986. Reconstitution of the hydrophobic core of low-density lipoprotein. *Methods Enzymol.* **128:** 608–613.
24. Aikawa, K., T. Furuchi, Y. Fujimoto, H. Arai, and K. Inoue. 1994. Structure-specific inhibition of lysosomal cholesterol transport in macrophages by various steroids. *Biochim. Biophys. Acta.* **1213:** 127–134.
25. Handel-Fernandez, M. E., and D. M. Lopez. 2000. Isolation of macrophages from tissues, fluids, and immune response sites. *In* Macrophages—A Practical Approach. D. M. Paulnock, editor. Oxford University Press, Oxford, UK. 1–30.
26. Hart, H. E., and E. B. Greenwald. 1979. Scintillation proximity assay (SPA)—a new method of immunoassay. Direct and inhibition mode detection with human albumin and rabbit antihuman albumin. *Mol. Immunol.* **16:** 265–267.
27. Cook, N. D. 1996. Scintillation proximity assay: a versatile high-throughput screening technology. *Drug Discov. Today.* **1:** 287–294.
28. Krieger, M. 1999. Charting the fate of the "good cholesterol": identification and characterization of the high-density lipoprotein receptor SR-BI. *Annu. Rev. Biochem.* **68:** 523–558.
29. Kodama, T., M. Freeman, L. Rohrer, J. Zabrecky, P. Matsudaira, and M. Krieger. 1990. Type I macrophage scavenger receptor contains alpha-helical and collagen-like coiled coils. *Nature.* **343:** 531–535.
30. Brown, M. S., J. L. Goldstein, M. Krieger, Y. K. Ho, and R. G. Anderson. 1979. Reversible accumulation of cholesteryl esters in macrophages incubated with acetylated lipoproteins. *J. Cell Biol.* **82:** 597–613.
31. Scriver, C. R., A. L. Beaudet, D. Valle, and W. S. Sly, editors. 2001. The Metabolic and Molecular Bases of Inherited Disease. McGraw-Hill, New York.
32. Mimura, N., and A. Asano. 1976. Synergistic effect of colchicine and cytochalasin D on phagocytosis by peritoneal macrophages. *Nature.* **261:** 319–321.
33. de Oliveira, C. A., and B. Mantovani. 1988. Latrunculin A is a potent inhibitor of phagocytosis by macrophages. *Life Sci.* **43:** 1825–1830.
34. Malawista, S. E., J. B. Gee, and K. G. Bensch. 1971. Cytochalasin B reversibly inhibits phagocytosis: functional, metabolic, and ultrastructural effects in human blood leukocytes and rabbit alveolar macrophages. *Yale J. Biol. Med.* **44:** 286–300.
35. Desjardins, M., and G. Griffiths. 2003. Phagocytosis: latex leads the way. *Curr. Opin. Cell Biol.* **15:** 498–503.